

EPJ E

Soft Matter and
Biological Physics

EPJ.org
your physics journal

Eur. Phys. J. E (2013) **36**: 76

DOI 10.1140/epje/i2013-13076-1

Nanoscale protein dynamics: A new frontier for neutron spin echo spectroscopy

David J.E. Callaway, Bela Farago and Zimei Bu

edp sciences



 Springer

Nanoscale protein dynamics: A new frontier for neutron spin echo spectroscopy^{*}

David J.E. Callaway^{1,2,a}, Bela Farago³, and Zimei Bu^{1,b}

¹ Department of Chemistry, the City College of New York, New York, NY, 10031, USA

² New York University School of Medicine, New York, NY 10016, USA

³ Institut Laue-Langevin, Grenoble, France

Received 17 September 2012 and Received in final form 16 December 2012

Published online: 17 July 2013 – © EDP Sciences / Società Italiana di Fisica / Springer-Verlag 2013

Abstract. Recent studies show that neutron spin echo spectroscopy (NSE) can reveal long-range protein domain motions on nanometer lengthscales and on nanosecond to microsecond timescales. This unique capability of NSE provides new opportunities to understand protein dynamics and functions, such as how binding signals are propagated in a protein to distal sites. Here we review our applications of NSE to the study of nanoscale protein domain motions in a set of cell signaling proteins. We summarize the theoretical framework we have developed, which allows one to interpret the NSE data (Biophys. J. **99**, 3473 (2010) and Proc. Natl. Acad. Sci. USA **102**, 17646 (2005)). Our theoretical framework uses simple concepts from nonequilibrium statistical mechanics, and does not require elaborate molecular dynamics simulations, complex fits to rotational motion, or elastic network models. It is thus more robust than multiparameter techniques that require untestable assumptions. We also demonstrate our experimental scheme involving deuterium labeling of a protein domain or a subunit in a protein complex. We show that our selective deuteration scheme can highlight and resolve specific domain dynamics from the abundant global translational and rotational motions in a protein. Our approach thus clears significant hurdles to the application of NSE for the study of protein dynamics in solution.

1 Nanoscale protein dynamics: The emergence of a new frontier

Protein dynamics is essential to all aspects of protein function, such as protein stability, enzyme catalysis, and the propagation of allosteric signals [1–3]. Protein dynamics is hierarchical, occurring on many orders of timescales and multiple lengthscales [4,5]. Biologically relevant protein motions occur on timescales ranging from femtoseconds to seconds. Neutron scattering can study dynamics from picosecond to microsecond timescales and on various lengthscales from angstroms to microns, which is an advantage of neutron scattering compared to other experimental techniques [6–11].

Nanoscale protein dynamics is emerging as a powerful paradigm for understanding protein function and cell signaling [12,13]. There is increasing evidence that the functions of proteins and macromolecular machines are dictated by protein dynamics on nanometer lengthscales and on nanosecond-to-microsecond timescales [14–17]. How-

ever, it is a challenge to study nanoscale protein dynamics experimentally because of the large size and heterogeneous nature of protein complexes. Currently there is an important *information gap*, on nanoscales, between the dynamics occurring at atomic resolution and the cellular organization and dynamics on the much larger micron lengthscales and slower timescales.

One technique can fill this information gap—neutron spin echo spectroscopy (NSE) [18,19]. In particular, NSE can determine protein dynamics on nanometer-to-micron lengthscales and on nanosecond-to-microsecond timescales. Recent studies show that NSE can reveal long-range protein domain motions on nanometer lengthscales and on nanosecond-to-microsecond timescales [20–22]. This unique capability of NSE provides new opportunities to understand protein dynamics and functions, such as how binding signals are propagated in a protein to distal sites. Such nanoscale protein dynamics influences protein-ligand binding, protein complex formation, and signal transduction.

Here we review our application of NSE to the study of nanoscale dynamics in a multidomain signaling protein as it forms protein complexes [20–22]. We summarize our new theoretical framework, which allows one to interpret the NSE data. Our theoretical framework uses simple concepts

^{*} Contribution to the Topical Issue “Neutron Biological Physics”, edited by Giovanna Fragneto and Frank Gabel.

^a e-mail: dcallaway@ccny.cuny.edu

^b e-mail: zbu@ccny.cuny.edu

from nonequilibrium statistical mechanics, and does not require elaborate molecular dynamics simulations, complex fits to rotational dynamics, or elastic network models. It is thus more robust than multiparameter techniques that require untestable assumptions. We also describe our experimental scheme of deuterium labeling of a protein domain or a subunit in a protein complex. We show that this selective deuteration scheme can highlight and resolve the specific domain motions from the plethora of global translational and rotational motions that are hurdles to the application of NSE to study protein dynamics in solution.

2 The nature of nanoscale protein dynamics

Nanoscale protein motions obey Brownian dynamics, and are overdamped rather than underdamped oscillations. Protein dynamics arises as a result of thermal forces from the collision of the protein with solvent molecules. These thermal forces are random in magnitude and direction, and lead to a protein undergoing a process known as Brownian motion or *diffusion*. A particle undergoing Brownian motion displays frequent changes in the direction and speed of its movement. The world in which proteins operate is therefore characterized by the presence of a significant amount of noise and the resultant diffusion of protein subunits arising from thermal motion. Thermal motions are essential for the protein to reach its equilibrium state.

The environment in which proteins act is one of low Reynolds number (usually abbreviated Re). Reynolds number (which was actually introduced by Stokes!) is the ratio of the magnitude of inertial forces to that of the thermal forces that arise from the viscous drag that opposes motion,

$$\text{Re} = Lv/\nu,$$

where L is a characteristic lengthscale of the protein, v is a characteristic velocity, and ν is the kinetic viscosity of the solvent (for water, $\nu \sim 10^5 \text{ \AA}^2/\text{ns}$). For a large object, inertial forces are more important than viscous drag. When Reynolds number is large, forces are proportional to mass times acceleration, according to Newton's second law. For a small particle such as a protein, viscous drag is more important and Reynolds number is small and forces are proportional to the velocity of the protein, incorporating a concept known as the mobility tensor that we will discuss in detail below. At large Reynolds number, one has oscillatory (underdamped) phenomena such as the ringing of a bell, while at small Re (which occurs when Re is less than about 2500), dynamics involves slow, creeping *overdamped* motion.

Reynolds number is actually an imprecise concept, usually used as a way to argue that certain terms in the Navier-Stokes equations of fluid dynamics can safely be neglected. Reynolds numbers for typical proteins are less than 0.1, indicating that protein dynamics is well within the low Re regime. Even a multiprotein complex as large as a ribosome is still within the overdamped regime [24].

The environment of a protein has more in common with playing badminton at the bottom of a swimming pool full of molasses (low Re) than a cruise ship crossing the Atlantic Ocean (high Re) [24]. For proteins, inertial forces are less important than diffusive and viscous effects, and protein dynamics should be largely independent of the mass of the protein (or of the relative masses of internal domains). Thus, the diffusion constant of a deuterated protein should be the same as a hydrogenated protein, even though deuterium has twice the mass of hydrogen, as we observe. This effect is an advantage for applying selective deuterium labeling and contrast matching in NSE.

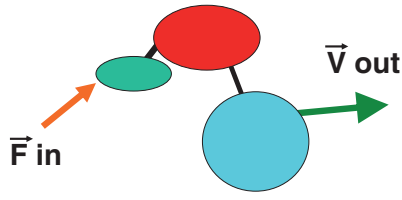
3 A new theoretical framework for extracting nanoscale protein dynamics from NSE experiments

Concomitant with the rise of NSE experiments to study protein dynamics, it becomes apparent that there is a need for developing a theoretical strategy in order to interpret the experimental results. The framework that we developed emerges as an extension, albeit more complex [20–22], of ideas developed for polymer dynamics [25,26]. We summarize the basic approach here. We begin by considering the dynamics information obtained via an NSE experiment. NSE measures the intermediate scattering function $I(Q, t)$, which is the spatial Fourier transformation of the space-time van Hove correlation function $G(r, t)$ [18], $I(Q, t) = \int_V G(r, t) \exp(-iQ \cdot r) dr$, with Q the magnitude of the scattering vector, t the time, and r the position of a scattering center. The designation “intermediate” arises precisely because only one of the variables of $G(r, t)$ is Fourier transformed. Like the static small angle neutron scattering, in the low Q region, $I(Q, t)$ is dominated by coherent scattering that corresponds to the cross-correlation $G(r, t)$, *i.e.*, the probability of finding a nucleus at position r_i at time $t = 0$ and finding another nucleus at position r_j at time t . For a protein in solution, $I(Q, t)$ can typically be fit to a single exponential in time (and is difficult to fit to more exponentials) at a given Q . A natural way to interpret the NSE data is to examine the effective diffusion constant $D_{\text{eff}}(Q)$ as a function of Q , which is determined by the normalized intermediate scattering function $I(Q, t)/I(Q, 0)$,

$$\begin{aligned} \Gamma(Q) &= -\lim_{t \rightarrow 0} \frac{\partial}{\partial t} \ln[I(Q, t)/I(Q, 0)], \\ D_{\text{eff}}(Q) &= \frac{\Gamma(Q)}{Q^2}, \end{aligned} \quad (1)$$

where $I(Q, 0)$ is the static form factor.

In order to describe the dynamics of a protein in solution, we utilize the remarkable Akcasu-Gurol (AG) approach originally developed to describe the dynamics of random coil polymers [27], which is generalized to include



Mobility tensor $\vec{v} = \vec{H} \vec{F}$

Fig. 1. The relationship between force, velocity, and the mobility tensor. The translational mobility tensor gives the velocity response (speed and direction) of a given protein domain to a force applied to itself or to another domain.

rotational motion [20],

$$D_{\text{eff}}(Q) = \frac{k_B T}{Q^2} \times \frac{\sum_{jl} \langle b_j b_l (Q \cdot H_{jl}^T \cdot Q + L_j \cdot H_{jl}^R \cdot L_l) e^{iQ \cdot (r_j - r_l)} \rangle}{\sum_{jl} \langle b_j b_l e^{iQ \cdot (r_j - r_l)} \rangle}, \quad (2)$$

where b_j is the coherent scattering length of a subunit j , H^T is the translational mobility tensor, H^R is the rotational mobility tensor; and $k_B T$ is the usual temperature factor. The structural coordinates of the macromolecule, taken relative to the center of friction of the protein, are given by \mathbf{r}_j (note that $\sum \mathbf{r}_j = 0$). In practice, the structural coordinates can be atoms, protein domains in a multidomain protein, or subunits in a multimeric protein complex, and may be obtained from high-resolution crystallography or NMR, or from low-resolution electron microscopy and small angle X-ray and neutron scattering. In eq. (2), $\mathbf{L}_j = \mathbf{r}_j \times \mathbf{Q}$ is the angular momentum vector for each coordinate. The brackets $\langle \rangle$ denote an orientational average over the vector \mathbf{Q} , so that $\langle Q_a Q_b \exp(i\mathbf{Q}\mathbf{r}) \rangle Q^{-2} = (1/3)\delta_{ab} j_0(Qr) + [(1/3)\delta_{ab} - (r_a r_b / r^2)] j_2(Qr)$ can be expressed in terms of the spherical Bessel functions j . The translational mobility tensor H^T in eq. (2) is defined by the velocity response $\mathbf{v} = H^T \mathbf{F}$ to an applied force \mathbf{F} . The rotational mobility tensor H^R is defined by the angular velocity response $\boldsymbol{\omega} = H^R \boldsymbol{\tau}$ to an applied torque $\boldsymbol{\tau}$. The relationship between force, velocity and the translational mobility tensor is illustrated in fig. 1.

The mobility tensor provides a direct indication of the existence of internal degrees of freedom. Equation (2) is valid for either rigid bodies or rigid-body subunits connected by soft spring linkers [20]. For a completely flexible body, the rotational diffusion term (involving H^R) is absent. The rotational mobility tensor arises from the consideration of rigid-body constraints, introduced via Lagrange multipliers or by generalized coordinates [25]. For a rigid body composed of N identical beads, the translational mobility tensor H^T is a matrix with N^2 identical 3×3 elements since H^T yields the same velocity response of, e.g., subunits B and C to a force applied to subunit A. For an object with internal flexibility, the elements of the mobility tensor will not be equal, so forces applied to

a given bead would result in different velocities for other beads and the body would not remain rigid. Comparing models of the mobility tensor from eq. (2) to experimental $D_{\text{eff}}(Q)$ from NSE experiments allows one to extract the internal dynamics of a protein or protein complex. Thus, the key point of eq. (2) is that the effective diffusion constant $D_{\text{eff}}(Q)$ can be calculated if we know the structural coordinates of the protein, and have proposed a model for the mobility tensor. NSE therefore allows us to test models of the mobility tensor, and thereby determine and characterize internal dynamic modes in the protein.

The angular velocity vector of the rigid object is $\boldsymbol{\omega} = H^R \boldsymbol{\tau}$, with the torque $\boldsymbol{\tau} = \sum_n \mathbf{r}_n \times \mathbf{F}_n$. The vector force \mathbf{F}_n on bead n is given in terms of the velocity \mathbf{v}_n and the overall angular velocity. Thus for an arbitrary 3-component vector $\boldsymbol{\omega}$

$$\boldsymbol{\omega} = H^R \sum_{mn} \mathbf{r}_m \times (N^2 H^T)^{-1}_{mn} (\boldsymbol{\omega} \times \mathbf{r}_n). \quad (3)$$

We note that eq. (3) is of the form $\boldsymbol{\omega} = M \boldsymbol{\omega}$ for an arbitrary vector $\boldsymbol{\omega}$, and thus M is the identity matrix. Equation (3) shows that for a rigid body the 3×3 matrix H^R can be evaluated by an inversion of a 3×3 matrix calculated by summing over bead coordinates n . The rotational mobility tensor is thus entirely determined by the translational mobility tensor and the coordinates of the protein. We adopt the simplifying assumption that all three principal spatial components of the translational mobility tensor for each subunit are equal to $N D_0 / (k_B T) = 1/\zeta$ with ζ the friction constant of a subunit, and D_0 the measured diffusion constant of the protein. Then a compact formula of H^R is given [21, 22],

$$H^R_{\alpha\beta} = N(D_0/k_B T) [\sum_n (\delta_{\alpha\beta} r_n^2 - r_{\alpha} r_{n\beta})]^{-1}, \quad (4)$$

where D_0 is the diffusion constant of the protein or protein complex at $Q = 0$, which can be measured experimentally by PFG NMR or dynamic light scattering, and N is the number of structural coordinates of the protein, relative to the center of friction (note that $\sum_n \mathbf{r}_n = 0$). With eqs. (2)–(4), an estimate of $D_{\text{eff}}(Q)$ for a rigid body can be made by simply using only the coordinates and the diffusion constant D_0 . There is therefore no need for a multiparameter molecular dynamics simulation or an elastic network model.

In general, both the rotational and translational mobility tensors have different values for each of the three principal axes, so that there are six independent quantities for each domain. In a multidomain protein complex, there are generally at least 24 independent quantities for the mobility tensor (3 translational plus 3 rotational for each of the four subunits). These quantities are difficult to evaluate to the precision required to compare with NSE data [23]. By contrast, in our calculation of H^R , we assume that the x , y , and z diagonal components of H^T are equal for each subunit and are the only nonzero components. Our simple approach requires neither complicated molecular dynamics simulations nor Navier-Stokes hydrodynamics.

For an object with internal domain motion, comparing the calculated $D_{\text{eff}}(Q)$ with experimental NSE data

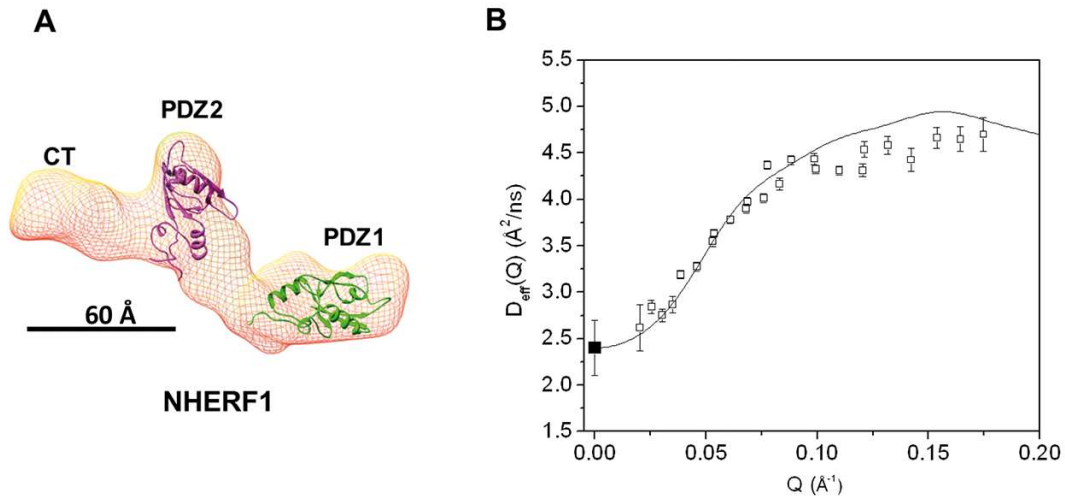


Fig. 2. Comparing experimental NSE results with theoretical calculations for NHERF1 alone. (A) The 3D shape of NHERF1 reconstructed from SAXS [31] using the *ab initio* program DAMMIN [32]. The known high-resolution structures of the PDZ1 (PDB code: 1I92) and PDZ2 (PDB code: 2KJD) domains are docked into the 3D shape, using UCSF Chimera [34]. EBD, which overlaps with the last 13 amino acid residues that interact with PDZ2 is not marked in the graph. (B) Comparing the experimental $D_{\text{eff}}(Q)$ of NHERF1 (black open square) with the rigid-body calculation (black solid line). The overall translational diffusion constant D_0 (filled black square) at $Q = 0 \text{ \AA}^{-1}$ is $D_0 = 2.4 \text{ \AA}^2/\text{ns}$ from PFG NMR measurements.

allows one to extract the relative degree of dynamic coupling between the various components of the system. This dynamic coupling is defined by the mobility tensor. For example, a rigid two-domain system is described by a mobility tensor,

$$H = H_0 \begin{pmatrix} 1 & 1 \\ 1 & 1 \end{pmatrix}, \quad (5a)$$

with all elements of the tensor equal, and yields (via eq. (2)) the simple result that the translational contribution to the effective diffusion constant is given by $D_{\text{eff}}^T(Q) = k_B T H_0$, independent of Q . By contrast, a two-domain system with internal motion will possess a mobility tensor,

$$H = \begin{pmatrix} H_1 & 0 \\ 0 & H_2 \end{pmatrix}, \quad (5b)$$

in principal coordinates. Thus, the application of equal forces to the two domains will result in their having different velocities, revealing internal motion. For the case where there is one internal translational mode between subunits 1 and 2 with $D_1 = k_B T H_1$ and $D_2 = k_B T H_2$ [20], the translational contribution to the effective diffusion constant is

$$D_{\text{eff}}^T(Q) = \frac{D_1 S_1(Q) + D_2 S_2(Q)}{S(Q)}. \quad (5c)$$

Here, $S_1(Q)$ and $S_2(Q)$ are the form factors of the separate individual protein domains, while $S(Q)$ is the form factor of the entire protein. Orientational averages are performed, so that, *e.g.*, $S(Q) = \sum j_0(Qr)$; and $S(Q)$ is normalized so that $S(0) = N^2$. D_1 and D_2 are the diffusion constants of individual domains.

To summarize, the calculations that we have presented consist of rigid-body motion (including both translational

and rotational motion), and an internal mode. We stress that, in principle, it is possible to include the effects of arbitrary translational and rotational internal motion in the calculation [20]. The combination of NSE and first cumulant analysis allows one to test complex models of the mobility tensors of the system, and extract dynamical information about the internal motions of the protein. *No other technique can do this.*

4 Applying NSE to the study of nanoscale protein motion

The virtue of the above simple approach can be seen by comparing our calculations with the experimental NSE results from a cell signaling a scaffolding protein called NHERF1 [21]. NHERF1 plays essential roles in modulating the intracellular trafficking and assembly of a number of receptors and ion transport proteins. NHERF1 is a multidomain protein that has two modular domains, PDZ1, PDZ2, and a disordered but compact C-terminal (CT) domain, with three domains connected by unstructured linkers [28–30]. The CT domain binds to the FERM domain of ezrin with high affinity with $K_d = 19 \text{ nM}$. We have shown that binding to FERM-binding to the CT domain allosterically increases the binding affinity of both PDZ1 and PDZ2 domains of NHERF1 for the cytoplasmic tail of CFTR [28,31]. The PDZ1 and PDZ2 domains are 110 Å and 80 Å away, respectively, from the FERM binding site in the CT domain. The NHERF1-FERM complex thus shows long-range allosteric transmission of binding signals on nano lengthscales.

For NHERF1 alone in solution, the calculated rigid body $D_{\text{eff}}(Q)$, using eqs. (2), (3), and (5a), agrees with

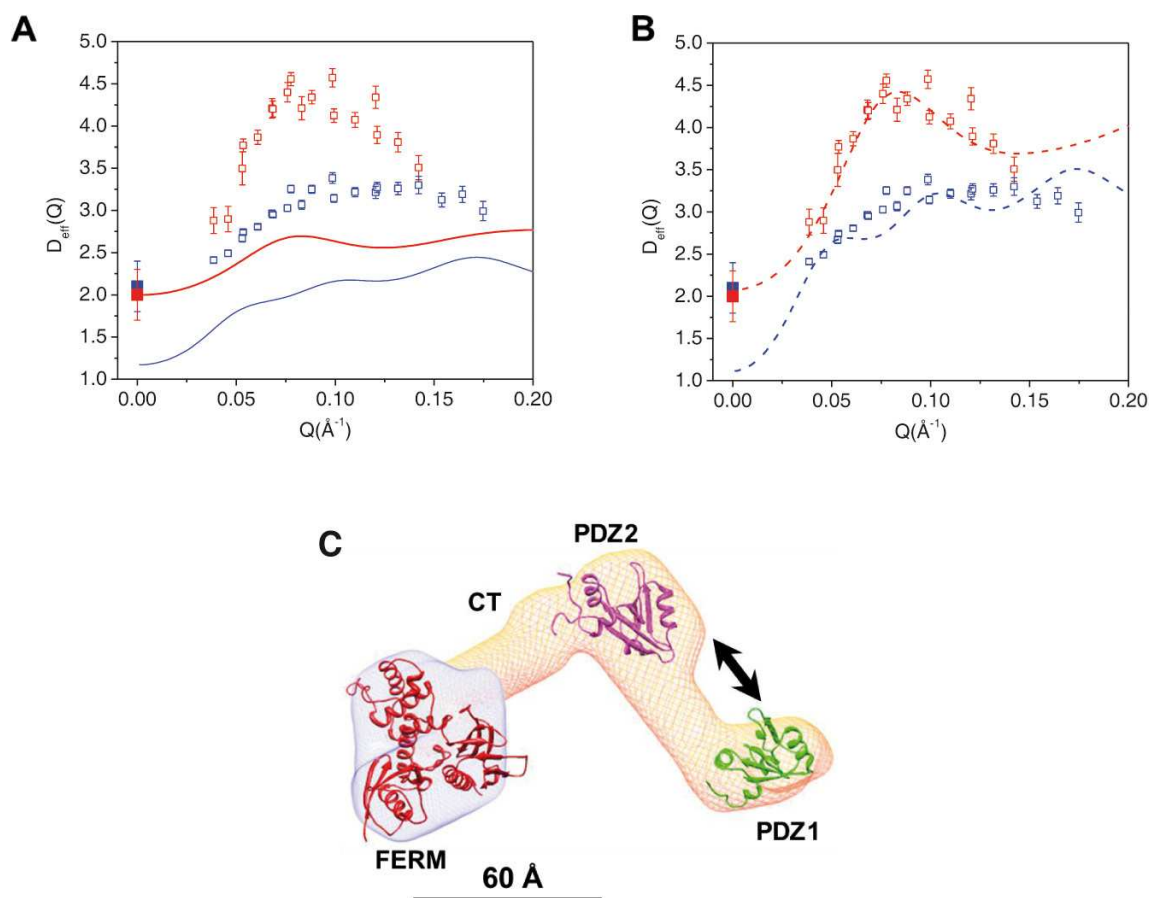


Fig. 3. Deuteration of the FERM domain amplifies the effects of protein internal motions detected by NSE. (A) Comparing experimental $D_{\text{eff}}(Q)$ of NHERF1-^dFERM and NHERF1-^hFERM with rigid-body calculations. Open red squares are the NSE data from NHERF1-^dFERM. Open blue squares are the NSE data from NHERF1-^hFERM. Solid red and blue squares are the self-diffusion constants D_0 of NHERF1-^dFERM and NHERF1-^hFERM obtained from PFG NMR, respectively. The solid red line is from rigid-body model calculations of the NHERF1-^dFERM complex. The solid blue line is from rigid-body model calculations of the NHERF1-^hFERM complex. (B) Comparing experimental $D_{\text{eff}}(Q)$ of deuterated complex NHERF1-^dFERM and hydrogenated complex NHERF1-^hFERM with calculations incorporating interdomain motion between PDZ1 and PDZ2. The symbols for the experimental data are the same as in (A). The dashed red curve is calculated from model incorporating domain motion between PDZ1 and PDZ2 for the NHERF1-^dFERM complex. The dashed blue curve is calculated from a model incorporating domain motion between PDZ1 and PDZ2 for the NHERF1-^hFERM complex. The comparisons in (A) and (B) show that deuteration of the FERM domain amplifies the effects of protein internal motions detected by NSE. (C) A model representing domain motion between PDZ1 and PDZ2 in the complex. The 3D shape of the complex is reconstructed from SANS [31]. The known high-resolution structure fragments of PDZ1, PDZ2, and ezrin FERM domain (PDB code: 1NI2) are docked into the envelope using UCSF Chimera [34]. The arrows represent translational motion between PDZ1 and PDZ2. A lengthscale bar of 60 Å is shown.

the NSE experimental data quite well, see fig. 2. The rigid-body calculation uses as input only the translational diffusion coefficient D_0 of NHERF1 obtained from pulsed-field gradient NMR and the “dummy atom” structural coordinates [32] reconstructed from solution small angle X-ray scattering (SAXS) [29,31].

We have compared our calculations with the NSE experimental results on two types of complexes of NHERF1 bound to FERM, see fig. 3. Figure 3A compares the experimental NSE data with rigid-body calculations. One is the hydrogenated NHERF1 in complex with the hy-

drogenated FERM (NHERF1-^hFERM), and the other is hydrogenated NHERF1 bound to deuterium labeled FERM (NHERF1-^dFERM). As we have pointed out, at low Reynolds number, the dynamics of a protein as seen by NSE should not depend upon its mass, but rather upon its size. In our calculations, we thus always impose the constraint that the dynamics (and therefore the mobility tensors) of the hydrogenated and deuterated components are the same. When calculating $D_{\text{eff}}(Q)$ for the NHERF1-^dFERM complex, the scattering from the deuterated component is treated as “invisible” in

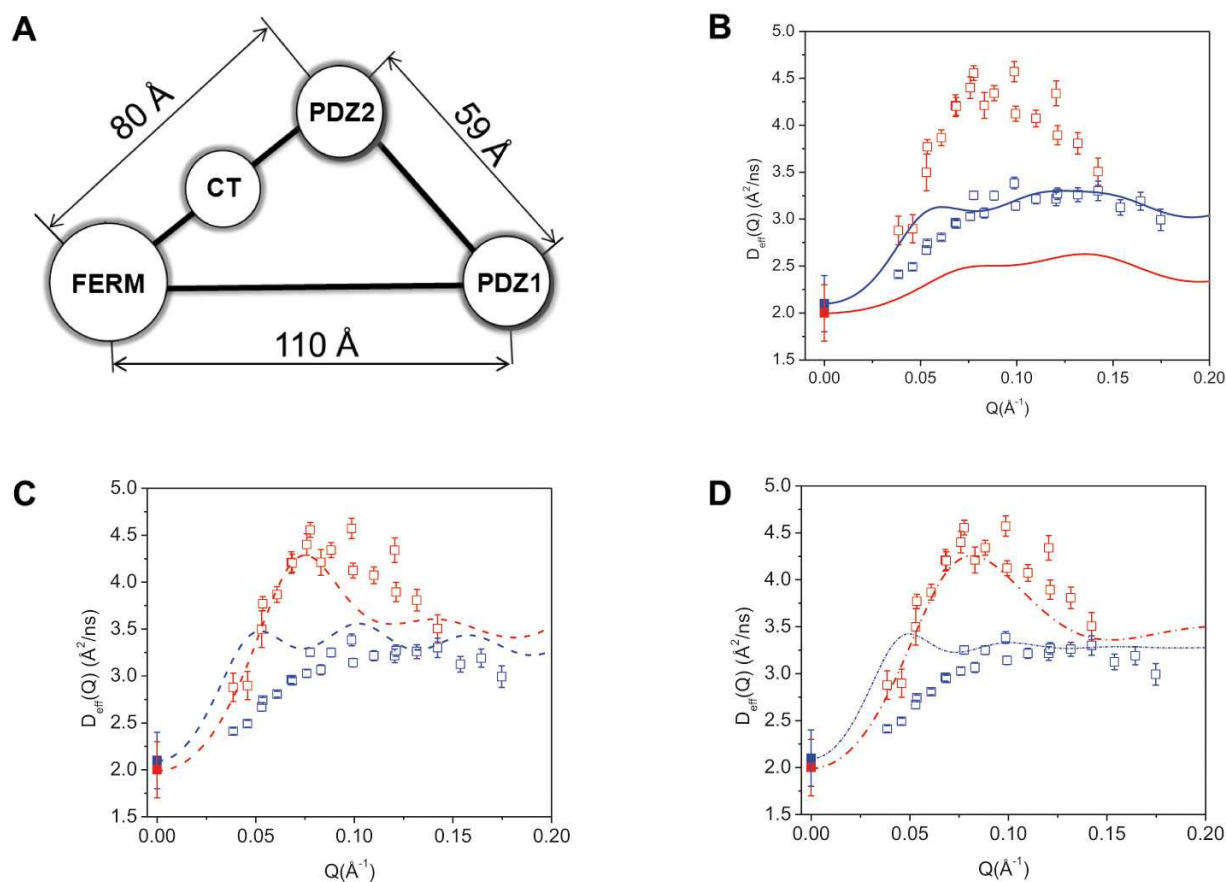


Fig. 4. A simple four-point model can well describe domain motion in the complex. (A) The four-point model represents the NHERF1-FERM complex, with the centers of PDZ1, PDZ2, CT, and FERM domain taken from fig. 3A. (B) Comparing the experimental NSE data with the four-point rigid-body calculations for NHERF1.^hFERM (blue open squares are the experimental data and blue solid line is the calculated data) and for NHERF1.^dFERM (red open squares are experimental data and red solid line is the calculated data). D_0 of NHERF1.^dFERM (solid red squares) and NHERF1.^hFERM (solid blue squares) from PFG NMR are shown. (C) Comparing the experimental data with calculations assuming inter-domain motion between PDZ1 and PDZ2 in NHERF1.^dFERM (red dash line) and NHERF1.^hFERM (blue dash line). The experimental symbols are the same as in (B). (D) Comparing the experimental data with calculations incorporating inter-domain motion between PDZ1 and PDZ2, as well as assuming finite size form factor of spheres of 20 Å radius for the FERM domain and for both PDZ domains in NHERF1.^dFERM (red dash dot line) and in NHERF1.^hFERM (blue dash dot line).

eq. (2) because the neutron scattering length density of the deuterated component contrast matches that of the D_2O buffer background. Similar to the calculations on NHERF1 alone, we used D_0 of the complexes obtained from PFG NMR and the structural coordinates obtained from SANS.

As shown in fig. 3A, the agreement between the experimental NSE data and *rigid-body* calculations is poor for both the NHERF1.^dFERM and the NHERF1.^hFERM complexes. We have then incorporated domain motions in our calculations, with the mobility tensor with an internal mode between the PDZ1 and PDZ2 domains (fig. 3B). The calculated $D_{\text{eff}}(Q)$ with internal motion agrees quite well with the NSE results for the NHERF1.^dFERM complex. Nevertheless, for the NHERF1.^hFERM complex, the computed D_0 at $Q = 0$ is not close to the experimental values

from PFG NMR measurements. We attribute this discrepancy to large conformational variations in NHERF1 by the unfolding of the CT domain upon binding to FERM [30], which cannot be represented by a single structure reconstructed from SANS. Such complications are minimal in the NHERF1.^dFERM complex because the deuterated ^dFERM is “invisible” to neutrons.

A simple four-point model describes the domain motion.

The simple calculations we presented above require only the structural coordinates and a single constraint, the diffusion constant at $Q = 0 \text{ \AA}^{-1}$ for the deuterated complex, which can be measured by PFG NMR, to generate the computed $D_{\text{eff}}(Q)$. We further introduce an even more simplified model that yields the same effect, and serves to explain the $D_{\text{eff}}(Q)$ observed by NSE experi-

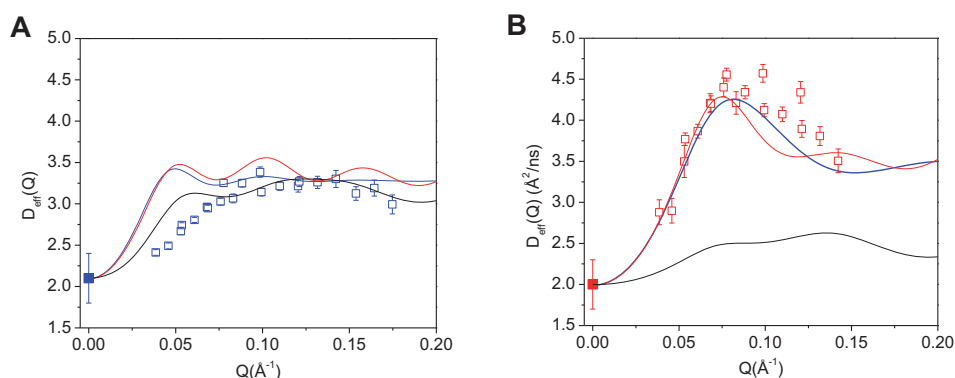


Fig. 5. For the hydrogenated NHERF1.^hFERM complex, the difference in $D_{\text{eff}}(Q)$ between the rigid-body model and domain-motion models is very small, but is significantly increased in the deuterated complex. (A) Comparing the rigid-body calculation with the domain-motion calculation in the four-point model in the hydrogenated NHERF1.^hFERM complex. NSE data from the NHERF1.^hFERM (blue open squares), the four-point rigid-body model (black line), four-point model incorporating domain motion between PDZ1 and PDZ2 (red line), four-point model incorporating domain motion between PDZ1 and PDZ2 and finite size form factor of 20 Å radius for the FERM domain, PDZ1 and PDZ2 (blue line). D_0 at $Q = 0 \text{ \AA}^{-1}$ as measured from PFG NMR is shown in blue solid square. (B) Comparing the rigid-body calculation with the domain-motion calculation in the four-point model in the deuterated NHERF1.^dFERM complex. NSE data from the NHERF1.^dFERM (red open squares), the four-point rigid-body model (black line), four-point model incorporating domain motion between PDZ1 and PDZ2 (red line), four-point model incorporating domain motion between PDZ1 and PDZ2 and finite size form factor of 20 Å radius for the FERM domain, PDZ1 and PDZ2 (blue line). D_0 at $Q = 0 \text{ \AA}^{-1}$ as measured from PFG NMR is shown in red solid square.

ments. The simplified model is taken by extracting four points that represent the coordinates of the center of *friction* of domains obtained from the SANS data of the NHERF1-FERM complex. These points form a triangle, as shown in fig. 4A, with the distances FERM-PDZ2 = 80 Å, PDZ2-PDZ1 = 59 Å, and FERM-PDZ1=110 Å. The CT domain is taken as being halfway between the FERM and PDZ2 domains. We include the point representing the FERM domain with a weight factor of 3 to account for its larger size relative to the other domains. Because it is possible to obtain the center-of-friction distances between the domains with confidence even with low resolution SAXS or SANS data, this model possesses fewer uncertainties than a model based upon the molecular shape. More details of the four-point calculations are described previously [21].

Figure 4B is the $D_{\text{eff}}(Q)$ of the four-point rigid-body model, without incorporating internal domain motion between PDZ1 and the rest of the complex. Figure 4C is the $D_{\text{eff}}(Q)$ of the four-point model incorporating internal domain motion between PDZ1 and the rest of the complex. After incorporating internal motion, the overall $D_{\text{eff}}(Q)$ from the four-point model agrees well with the experimental data for both the partially deuterated and the hydrogenated complexes. The comparison between calculation and experimental data improves after including the form factor of a 20 Å radius sphere for the FERM domain and both PDZ domains in the calculation (fig. 4D). Thus, the NSE data is better represented by the four-point model that includes PDZ1-PDZ2 interdomain motion than by a model that assumes the complex is a rigid body. Further improvement likely requires the use of methods of evaluating the mobility tensors for proteins with high accuracy.

Moreover, from the four-point model calculations, we note that $D_{\text{eff}}(Q)$ for the hydrogenated rigid complex and

the hydrogenated complex with internal motion are nearly indistinguishable (fig. 5A). For the deuterated complex, $D_{\text{eff}}(Q)$ obtained from the inter-domain motion model is significantly different from that of the rigid-body model (fig. 5B). This can be explained as due to the relatively large contribution to eq. (2) of the effects of rotational diffusion of the overall object, which dominates and obscures the effects of internal motion when no deuteration is performed. For the partially deuterated complex, both the docked domain calculation (fig. 3B) and the four-point model (fig. 5B) show that $D_{\text{eff}}(Q)$ of the rigid-body complex is significantly different from that of the complex with internal domain motion. Thus, deuteration of a domain or subunit in a protein complex can amplify the effects of internal protein dynamics as detected by NSE.

5 Conclusions and perspectives

The above NSE experimental results and our calculations indicate that NHERF1 alone behaves as a rigid body on the timescale and lengthscales probed by NSE. Upon binding to FERM, interdomain motions between PDZ1 and PDZ2 become activated on nanosecond to submicrosecond timescales. The changes in nanoscale protein domain motion in the NHERF1-FERM complex correspond to long-range allostery in NHERF1, for FERM-binding to NHERF1 allosterically increases the ligand-binding affinities of both PDZ1 and PDZ2 of NHERF1 [28,31]. The results demonstrate the unique power of NSE to detect changes in nanoscale protein domain motions that correlate with protein functions, on such timescales and lengthscales that cannot be reached by other experimental techniques.

Much work remains to be done, however. The measurement of the diffusion constant for a protein suffers from the same difficulties as SAXS and SANS, namely that one can only determine a rotationally averaged result, and not the full 3×3 tensor. Numerical calculations do not provide much help, as estimates of even the overall diffusion constant are typically off by a factor of two or more. Moreover, for the above reason, there is no way to compare them with experiment. Also, structure reconstruction programs for SAXS and SANS typically include the assumption that the protein is convex, that is, that a line drawn between two points in the protein does not pass outside the protein. This may be fine for very globular proteins, but can lead to errors if the protein is an extended object, where dynamics is likely to be important [21,22]. Improvement in these methods would be highly useful.

As we have shown in both our NSE experiments and calculations, the problem of global rigid-body translational and rotational diffusion can be overcome by selective deuteration. Deuterium labeling of a domain in a protein or in a protein complex significantly amplifies the effects of internal motion detected by NSE. Thus, future NSE experiments should benefit by utilizing our strategy of selective deuteration to highlight the domain motions of interest.

Selective deuteration of a subunit in a complex can be performed by expressing the different components in hydrogenated and deuterated forms, respectively, and reconstituting the complex [21,31]. For a multidomain protein, selective deuteration of a domain or a segment may be achieved by the protein ligation methods for future NSE experiments [33,34]. Additionally, many mammalian signaling proteins must be expressed in insect cells or mammalian cells, in order to fold properly for function and for biophysical studies. The challenge is how to express isotope labeled proteins in insect or mammalian cells, at a reasonable cost, for neutron scattering experiments.

Protein motion on nanoscales is, at best, difficult to observe by other experimental techniques. The deuterium labeling approach and the theoretical analyses that we developed therefore should pave the way for using NSE to study protein motions in multidomain proteins. We expect NSE to fill an important spatial-temporal gap in our ability to characterize protein motion and function.

This work is supported by National Institutes of Health Grant R01 HL086496.

References

- G. Zaccai, *Science* **288**, 1604 (2000).
- A. Cooper, D.T.F. Dryden, *Eur. Biophys. J.* **11**, 103 (1984).
- S.J. Benkovic, S. Hammes-Schiffer, *Science* **301**, 1196 (2003).
- O. Miyashita, J.N. Onuchic, P.G. Wolynes, *Proc. Natl. Acad. Sci. U.S.A.* **100**, 12570 (2003).
- A. Mittermaier, L.E. Kay, *Science* **312**, 224 (2006).
- V. Receveur, P. Calmettes, J.C. Smith, M. Desmadril, G. Coddens, D. Durand, *Protein. Struct. Funct. Genet.* **28**, 380 (1997).
- V. Reat, H. Patzelt, M. Ferrand, C. Pfister, D. Oesterheld, G. Zaccai, *Proc. Natl. Acad. Sci. U.S.A.* **95**, 4970 (1998).
- M. Tehei, D. Madern, C. Pfister, G. Zaccai, *Proc. Natl. Acad. Sci. U.S.A.* **98**, 14356 (2001).
- F. Gabel, D. Bicout, U. Lehnert, M. Tehei, M. Weik, G. Zaccai, *Q. Rev. Biophys.* **35**, 327 (2002).
- Z. Bu, J. Cook, D.J. Callaway, *J. Mol. Biol.* **312**, 865 (2001).
- Z. Bu, D.A. Neumann, S.H. Lee, C.M. Brown, D.M. Engelman, C.C. Han, *J. Mol. Biol.* **301**, 525 (2000).
- B. Ma, C.J. Tsai, T. Haliloglu, R. Nussinov, *Structure* **19**, 907 (2011).
- R. Nussinov, *Mol. Biosyst.* **8**, 22 (2012).
- W. Wriggers, K. Schulten, *Protein. Struct. Funct. Genet.* **29**, 1 (1997).
- C. Xu, D. Tobi, I. Bahar, *J. Mol. Biol.* **333**, 153 (2003).
- P.I. Zhuravlev, G.A. Papoian, *Q. Rev. Biophys.* **43**, 295 (2010).
- D.L. Ho, W.M. Byrnes, W.P. Ma, Y. Shi, D.J. Callaway, Z. Bu, *J. Biol. Chem.* **279**, 39146 (2004).
- F. Mezei, in *Neutron Spin Echo: proceedings of a Laue-Langevin Institut workshop* (Springer, Heidelberg, 1980).
- B. Farago, in *Neutron Spin Echo Spectroscopy*, edited by F. Mezei, C. Pappas, T. Gutberlet, Vol. **601** (Springer, 2003) pp. 15 and B. Ewen, D. Richter, in *Neutron Spin Echo Spectroscopy Viscoelasticity Rheology*, Vol. **134** (1997).
- Z. Bu, R. Biehl, M. Monkenbusch, D. Richter, D.J. Callaway, *Proc. Natl. Acad. Sci. U.S.A.* **102**, 17646 (2005).
- B. Farago, J. Li, G. Cornilescu, D.J. Callaway, Z. Bu, *Biophys. J.* **99**, 3473 (2010).
- Z. Bu, D.J. Callaway, *Adv. Protein Chem. Struct. Biol.* **83**, 163 (2011).
- D. Richter, *J. Appl. Crystallogr.* **40**, s28 (2007).
- J. Howard, *Mechanics of Motor Proteins and the Cytoskeleton* (Sinauer Associates, Sunderland, MA, 2001).
- M. Doi, S.F. Edwards, *The Theory of Polymer Dynamics* (Oxford University Press, Oxford, 1986).
- B.J. Berne, R. Pecora, *Dynamic Light Scattering with Applications to Chemistry, Biology and Physics* (Dover Publications, Inc, Mineola, New York, 1976).
- Z. Akcasu, H. Gurul, *J. Polym. Sci. Part B Polym. Phys.* **14**, 1 (1976).
- J. Li, Z. Dai, D. Jana, D.J. Callaway, Z. Bu, *J. Biol. Chem.* **280**, 37634 (2005).
- J. Li, P.I. Poulidakos, Z. Dai, J.R. Testa, D.J. Callaway, Z. Bu, *J. Biol. Chem.* **282**, 27086 (2007).
- S. Bhattacharya, Z. Dai, J. Li, S. Baxter, D.J.E. Callaway, D. Cowburn, Z. Bu, *J. Biol. Chem.* **285**, 9981 (2010).
- J. Li, D.J. Callaway, Z. Bu, *J. Mol. Biol.* **392**, 166 (2009).
- D.I. Svergun, *Biophys. J.* **76**, 2879 (1999).
- T.W. Muir, D. Sondhi, P.A. Cole, *Proc. Natl. Acad. Sci. U.S.A.* **95**, 6705 (1998).
- R. Xu, B. Ayers, D. Cowburn, T.W. Muir, *Proc. Natl. Acad. Sci. U.S.A.* **96**, 388 (1999).
- E.F. Pettersen, T.D. Goddard, C.C. Huang, G.S. Couch, D.M. Greenblatt, E.C. Meng, T.E. Ferrin, *J. Comput. Chem.* **25**, 1605 (2004).